INORGANIC CHEMISTRY

FRONTIERS

Accepted Manuscript

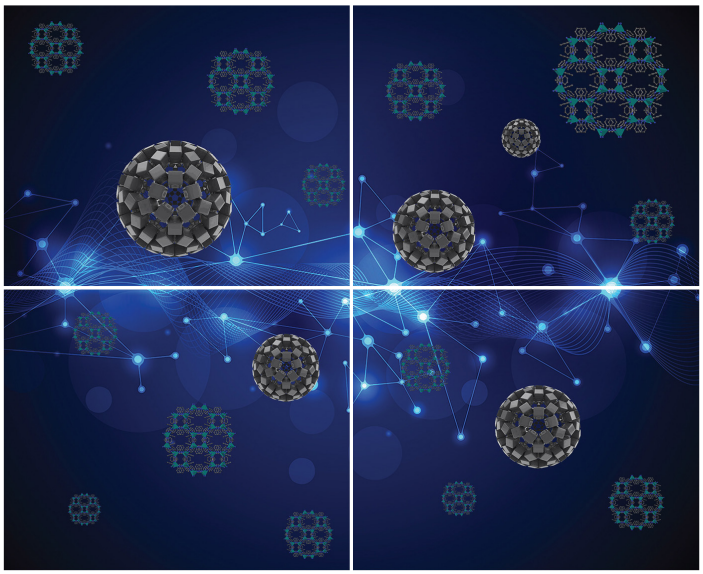

This article can be cited before page numbers have been issued, to do this please use: A. Brown, M. Cui, X. Feng, K. Singh, F. Ortu, H. Xiao and K. Suntharalingam, *Inorg. Chem. Front.*, 2026, DOI: 10.1039/D6QI00611F.

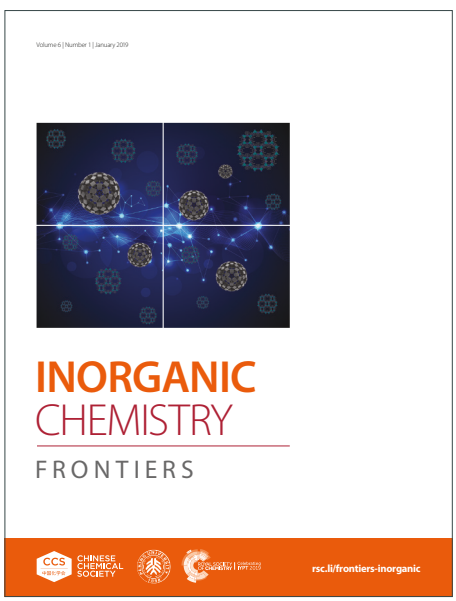

View Article Online
DOI: 10.1039/D6QI00611F

ARTICLE

A Necroptosis-Inducing Nickel(II) Complex for Immunotherapeutic Activation of Breast Cancer Stem Cells

Alex G. Brown,[†a] Minhui Cui,[†b] Xiao Feng,[†a] Kuldip Singh,[a] Fabrizio Ortu,*[a] Haihua Xiao*[b] and Kogularamanan Suntharalingam*[a]

Received 00th January 20xx,
Accepted 00th January 20xx

DOI: 10.1039/x0xx00000x

The immunotherapeutic anti-cancer stem cell (CSC) properties of a nickel(II) complex containing non-steroidal anti-inflammatory drug, diclofenac is reported. The nickel(II) complex **4** displays nanomolar potency towards breast CSCs, >264-fold greater than salinomycin (gold standard anti-breast CSC agent) and cisplatin (blockbuster anticancer metallodrug). In fact, **4** is more potent towards breast CSCs than any previously reported metal-containing compound. Notably, **4** exhibits significantly higher selectivity for breast CSCs over bulk breast cancer cells than salinomycin. Mechanistic studies suggest that **4** induces necroptosis and inhibits cyclooxygenase-2 expression (and thus perturbs the inhibitory damage-associated molecular pattern axis) in breast CSCs. Both factors contribute to an immunogenic phenotype in breast CSCs that does not exhibit all the hallmarks of immunogenic cell death. Further, breast CSCs dosed with **4** were efficiently phagocytosed by macrophages. Remarkably, when delivered as a polymeric nanoparticle formulation in a murine metastatic triple-negative breast cancer model, **4** significantly inhibits tumour growth and promotes immune system activation. The latter was characterised by T-cell and mature dendritic cell infiltration into the tumour and tumour-draining lymph nodes. To the best of our knowledge, **4** is among the first necroptosis-inducing metal complexes to evoke immunogenic-activating effects towards hard-to-kill breast cancer cells *in vitro* and *in vivo*.

Introduction

Advancements in cancer care have been hampered by tumour heterogeneity, and the existence of cancer cell sub-populations with phenotypical profiles that enable treatment resistance.[1] Cancer stem cells (CSCs) contribute to tumour heterogeneity, and have the ability to self-renew, differentiate, and promote secondary tumour formation.[2] The quiescent nature of CSCs coupled with their tendency to reside in hard-to-access areas, means they are elusive to chemotherapy and radiotherapy as well as surgical interventions.[3-7] After escaping conventional therapies, CSCs can reform tumours within the primary site or promote cancer cell motility and tumour anchorage at secondary sites.[8, 9] Given the negative clinical implications of CSCs, it is imperative that treatment regimens have the ability to remove heterogeneous tumour populations in their entirety, including CSCs, so the possibility of CSC mediated cancer reoccurrence is reduced. Immunotherapeutic approaches, that utilise the inherent cancer-fighting properties of the immune system, can provide durable anti-CSC therapeutic options.[10] In order to trigger a robust immune response against CSCs through the application of exogenous agents, the mode of cell death evoked needs to be carefully considered. The majority of chemotherapeutics in clinical use or development kill cancer cells by apoptosis.[11] Cytotoxic compounds can also kill cancer cells through non-apoptotic pathways, such as necroptosis.[12] Necroptosis is a regulated inflammatory mode of cell death that relies on the formation of an amyloid-like fibrillar complex called necrosome, consisting of receptor-interacting protein kinases 1 and 3 (RIP1 and RIP3), and a mixed-lineage kinase domain-like protein (MLKL).[13, 14] Recent studies showed that the induction of necroptosis in melanoma or adenocarcinoma mice models led to the recruitment and activation of cytotoxic T-cells, and thus a robust immune response with complete cancer regression and protection from subsequent tumour rechallenges.[15] Induction of apoptosis did not lead to immune system activation or tumour suppression.[15] Therefore, necroptosis-inducing agents could be used to trigger a robust immune response towards CSCs. The induction of necroptosis in CSCs is a completely unexplored strategy for immunotherapy.[16] It should be noted that although necroptosis can be used to immunogenically overcome apoptosis-resistant CSCs, it is highly inflammatory in nature and its induction is reliant on sufficient expression of the receptor-interacting protein kinases 1 and 3 (RIP1 and RIP3).[17] Therefore, the immunogenic potential of necroptosis-inducers could vary across tissue types.

A number of small molecule necroptosis-inducer have been identified in CSC and bulk cancer cell systems, including those containing metals, however very few have been investigated for their immunogenic potential.[18-25] A ruthenium(II) complex with 1,1-(pyrazin-2-yl)pyreno[4,5-e][1,2,4]triazine, bipyridyl, and phenylpyridyl ligands was reported to induce necroptosis via the inhibition of topoisomerase I and II activity in alveolar

[a] School of Chemistry, University of Leicester, Leicester, LE1 7RH, UK
[b] Beijing National Laboratory for Molecular Sciences, Laboratory of Polymer Physics and Chemistry, Institute of Chemistry Chinese Academy of Sciences, Beijing, 100190, P. R. China
E-mail: k.suntharalingam@leicester.ac.uk; fabrizio.ortu@leicester.ac.uk; hhxiao@iccas.ac.cn
† These authors contributed equally.

View Article Online
DOI: 10.1039/D6QI00611F

adenocarcinoma cells (the impact on alveolar-related CSCs was not investigated).[26] Another organoruthenium(II) complex with a triazene ligand was shown to induce necroptosis in colorectal adenocarcinoma cells by impacting mitochondrial function (the effect on colorectal CSCs was not evaluated).[27] Most notably, with respect to the CSC-focus of our study, osmium(II)- and ruthenium(II)-*p*-cymene complexes bearing bathophenanthroline and dichloroacetate ligands were reported to trigger necroptosis in breast CSCs.[18] We reported a nickel(II)-phenanthroline complex with dithiocarbamate ligands capable of killing both breast CSCs and osteosarcoma stem cells (OSCs) by necroptosis, in the micromolar range.[19, 20] Mechanistic studies revealed that the nickel(II) complex was able to evoke cell death by necrosome-mediated cell membrane disruption and mitochondrial depolarisation.[19, 20] Unbiased predictive functional genetic analysis based on RNA interference showed that the mechanism of action of the nickel(II) complex resembled that of shikonin, a *bona fide* necroptosis-inducer.[19] The functional outcome with respect to anti-CSC immunity of the nickel(II)-phenanthroline complex with dithiocarbamate was not explored. Structurally related nickel(II)-phenanthroline complexes with non-steroidal anti-inflammatory drugs (NSAIDs), namely naproxen, indomethacin, and flufenamic acid, were reported to kill breast CSCs and OSCs via necroptosis and cyclooxygenase-2 (COX-2) inhibition, in the micromolar range.[21, 22] Translation of these complexes was curtailed by limited solution stability and nickel leaching, a shortcoming that will be addressed in the current study. COX-2 is an enzyme that catalyses prostaglandin formation and is overexpressed in certain CSCs.[28] Prostaglandin was recently identified as an inhibitory damage-associated molecular pattern (iDAMP).[29] Immune cells are stimulated by bulk cancer cells and CSCs that have undergone immunogenic cell death (ICD) through the release of DAMPs.[30-32] iDAMPs can block ICD, therefore inhibition of COX-2 (and thus reduction in prostaglandin levels) in CSCs by exogenous agents can potentially promote ICD of CSCs. Recently we reported a cobalt(III)-cyclam complex with flufenamic acid that was able to perturb the iDAMP axis and thus induce an immunogenic response *in vitro* towards breast CSCs.[33] The cobalt(III)-cyclam complex evokes apoptosis as the mode of cell death (rather than necroptosis). The *in vivo* immunogenicity of the cobalt(III)-cyclam complex was not investigated.[33] In this study we have sought to combine the necroptosis-activating properties of the nickel(II)-phenanthroline moiety and the iDAMP-modulating properties of diclofenac (a NSAID)[34] to develop a stable coordination complex that can evoke outstanding immunogenic responses against chemotherapy-resistant breast cancer cells *in vitro* and *in vivo*. As far as we are aware this study is one of a few to explore the immunogenic potential of a nickel coordination complex in the context of anti-breast CSC therapeutics. There are significant translational challenges associated with nickel-based therapeutics, including systematic toxicity arising from the inherent reactivity of nickel coordination complexes, allergenicity associated to nickel-mediated immune system activation, and a lack of clinical precedent for nickel-based drug candidates in anticancer therapy. It should also be noted that within this research domain, very recently, a gold(III) complex with an isoquinoline-derived cyclometalated ligand and a dithiocarbamate ligand was shown to induce necroptosis and elicit necroptosis-dependent ICD *in vitro* and *in vivo* in murine colon adenocarcinoma models, however, the capacity to effect CSC populations was not explored.[35]

Results and Discussion

Synthesis and characterisation

A series of nickel(II)-polypyridyl complexes **1**-**4** appended to diclofenac were investigated in this study (Figure 1A). The nickel(II) complexes **1**-**4** were synthesised by reacting $NiCl_2{\cdot}6H_2O$ with two equivalents of sodium diclofenac and one equivalent of the corresponding polypyridyl ligand in methanol (see SI). The nickel(II) complexes **1**-**4** were fully characterised by infrared and UV-vis spectroscopy, high-resolution ESI mass spectrometry, and elemental analysis (Figures S1-S6). Analysis of the vibrational stretching frequencies associated to the asymmetric and symmetric carboxylato peaks provides insight into the binding mode of diclofenac in **1**-**4** to the nickel centre. The difference between the carboxylato peaks for **1**-**4** varied between 174-191 cm^{-1} (ν_{asym} C=O band varied from 1553-1575 cm^{-1} and ν_{sym} C=O band varied from 1377-1386 cm^{-1}, Figure S1), suggestive of a bidentate binding mode for diclofenac.[36, 37] The UV-vis spectra of **1**-**4** (1 mM, chloroform) displayed bands between 627-639 nm (ε varied from 7.2-25.2 M^{-1} cm^{-1}) corresponding to d-d transitions typical of nickel(II) octahedral complexes containing ligands with nitrogen and oxygen donor atoms (Figure S2).[38, 39] Distinctive molecular ion peaks with the appropriate isotopic pattern expected for **1**-**4** were observed in the high-resolution ESI mass spectra (Figures S3-S6). The purity of **1**-**4** was confirmed by elemental analysis. Single crystals of **2** suitable for X-ray diffraction analysis were obtained by layering a dichloromethane solution of **2** with pentane (Figure 1B, CCDC 2483096, Table S1-S2).[40] The complex exhibits a distorted

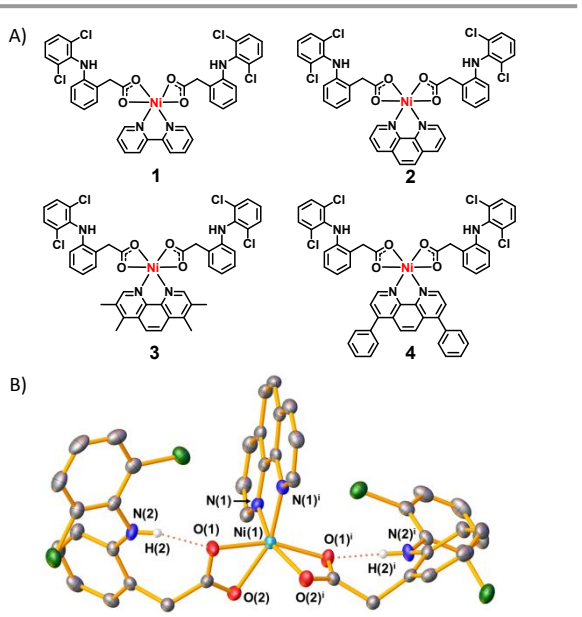

Figure 1. (A) Chemical structures of the nickel(II)-diclofenac complexes **1**-**4** under investigation in this study. (B) X-ray structure of **2** containing a distorted octahedral nickel(II) centre bound to 1,10-phenanthroline and two diclofenac units. The ellipsoids are set at the 30% probability level. Hydrogen atoms have been omitted for clarity, with the exception of atom H(2). Symmetry operation used to generate equivalent atoms: *i* = 1–*x*, +*y*, 3/2–*z*.

View Article Online
DOI: 10.1039/D6QI00611F

octahedral geometry with the nickel centre coordinated to 1,10-phenanthroline and two diclofenac molecules (via both carboxylato oxygen atoms). Analysis of long-range contacts reveals a hydrogen bonding interaction between one of the carboxylato oxygen atoms and the amine proton on diclofenac (O(1)···H(2), 2.013 Å); the hydrogen atom was clearly identified in the difference density map (Figure S7) and its position was refined freely. The crystal packing diagram for **2** is provided in Figure S8. This hydrogen bonding interaction could, in part, explain the preference of the diclofenac molecules to bind to the nickel centre in a bidentate manner and contribute to the overall stability of the complex.

Solubility and stability in biologically relevant solutions

The LogP values for **1**-**4** (determined by the shake-flask method) varied between 0.49 ± 0.004 and 1.89 ± 0.01, and were directly correlated to the bulkiness of the polypyridyl ligand present (Table S3). To investigate the stability of **1**-**4** in biologically relevant solutions, time course UV-vis spectroscopy and high-resolution ESI mass spectrometry studies were performed. Cell studies typically involve the preparation of stock solutions of the test compound in DMSO prior to dilution in cell culture media. Therefore, the UV-vis trace of **1**-**4** (25 μM) in DMSO and cell medium DMEM:DMSO (4:1) was monitored over the course of 24 h at 37 °C. The absorption bands associated to **1**-**4** remained largely unaltered in DMSO and DMEM:DMSO (4:1) indicative of good stability (Figures S9-S10). It should be noted, however, that the UV-vis trace of **4** (25 μM) in cell medium DMEM:DMSO (4:1) showed a slight decrease in absorption (21%) over the course of 24 h at 37 °C, which could be due to inherent instability under these conditions. Additional UV-vis spectroscopy studies in PBS:DMSO (200:1) with and without ascorbic acid or glutathione (cellular reductants), indicated that **1**-**4** (25 μM) were stable in biologically reducing conditions (Figures S11-S13). Time course ESI mass spectrometry studies with **4** (500 μM) in the presence of glutathione, cysteine, and lysine (10-fold excess) in H_2O:DMSO (5:1) at 37 °C over 72 h (Figures S14-S16) were conducted. Under all conditions, the ESI spectra displayed a distinctive signal for the corresponding molecular ion throughout the incubation period, implying that **4** remains intact (at least partially) in the presence of representative metal-coordinating biomolecules. The high-resolution ESI mass spectrum of **4** (500 μM) in H_2O:DMSO (5:1) was recorded after incubation for 24 h at 37 °C. The ESI mass spectra of **4** displayed a distinctive peak for the corresponding molecular ion (with the appropriate isotopic pattern) after the incubation period (Figure S17), indicating that **4** potentially remains intact in aqueous solution. Given that ionisation variability in ESI mass spectrometry can sometimes bias signal intensities or suppress certain species signals, the overall peak profile may not always reflect the true solution composition, and hence some caution must be taken when considering the conclusions raised from the ESI mass spectrometry stability data.

Further, HPLC analysis showed that when **4** (250 μM) was incubated in DMEM:DMSO (4:1) for 72 h at 37 °C, the complex stayed largely intact (98.9 %) with no sign of 4,7-diphenyl-1,10-phenanthroline liberation (Figures S18-S19). Stability experiments were also performed with human plasma. Upon incubation of **4** (500 μM) in human plasma for 72 h at 37 °C, the amount of intact **4** (unbound to proteins in human plasma), measured by UV-vis spectroscopy and ICP-MS analysis, remained largely unchanged (Figure S20, Table S4). This shows that **4** is potentially resistant to nickel leaching and structural modifications in human plasma over 3 days.

Monolayer and three-dimensional cytotoxicity towards breast cancer stem cells

The potency of **1**-**4** against bulk breast cancer cells (HMLER) and breast CSC-enriched cells (HMLER-shEcad) cultured in monolayer systems was determined using the MTT assay. HMLER cells are human mammary epithelial cells that have been immortalised and transformed by retroviral expression of SV40 large T oncogene, hTERT and H-rasV12. HMLER-shEcad cells are HMLER cells subjected to E-cadherin silencing by short hairpin RNA interference.[41] Breast CSCs have been characterised to display a $CD44^+/CD24^-$ phenotype[42] and the breast CSC population within the HMLER and HMLER-shEcad cell lines has been previously characterised by us and others and shown to display the appropriate $CD44^+/CD24^-$ phenotypes.[41, 43] HMLER cells exhibit a stable CSC-like population of 5-8 %, whereas HMLER-shEcad cells display a significantly larger CSC-like population (approximately 90 %).[41, 43] The half-maximal inhibitory concentrations (IC_{50}) were determined from dose-response curves (Figures S21-S24) and are summarised in Table 1. The nickel(II) complexes **1**-**4** exhibited micromolar to nanomolar toxicities towards HMLER and HMLER-shEcad cells with the 4,7-diphenyl-1,10-phenanthroline-containing complex **4** displaying the highest potency towards both cell lines. Strikingly, **4** exhibited 6.8-fold greater potency ($p < 0.05$, n = 18) for breast CSC-enriched HMLER-shEcad cells over CSC-depleted HMLER cells (Table 1). An inferior breast CSC versus bulk breast cancer cell selectivity profile was observed for salinomycin (2.7-fold, $p < 0.05$, n = 18, Table 1), a gold standard anti-breast CSC agent.[43] Remarkably, the breast CSC potency of **4** (IC_{50} value = 16 ± 1 nM) was significantly greater ($p < 0.05$, n = 18) than a panel of clinically approved breast cancer drugs (capecitabine, 5-fluorouracil, cisplatin, carboplatin), salinomycin, and any previously reported metal-containing agent (under identical conditions) (Table 1).[43-46] The most potent metal-containing compounds towards breast CSC-enriched HMLER-shEcad cells reported to date are the antirheumatic agent auranofin (IC_{50} = 26 ± 5 nM) and an Au(I) complex bearing triphenylphosphine and indomethacin (IC_{50} = 63 ± 6 nM).[45] It is difficult to pinpoint the reason for the extremely high potency of **4** towards HMLER and HMLER-shEcad cells, however, we believe it could be, in part, due to the ability of **4** to potentially induce necroptosis and the sensitivity of HMLER and HMLER-shEcad cells to necroptosis-inducing agents.[19, 21] The lipophilicity of **4** (LogP = 1.89 ± 0.01, Table S3) could also be playing a part by enabling passive uptake into HMLER and HMLER-shEcad cells.

Control cytotoxicity studies with the individual components of **4** were conducted. $NiCl_2{\cdot}6H_2O$, 4,7-diphenyl-1,10-phenanthroline, sodium diclofenac, and [Ni^{II}(4,7-diphenyl-1,10-phenanthroline)Cl_2] were significantly ($p < 0.05$, n = 18) less toxic (up to 728-fold) towards HMLER-shEcad cells than **4** (Figure S25, Table S5). The combined treatment of a 1:2 mixture of [Ni^{II}(4,7-diphenyl-1,10-phenanthroline)Cl_2] and sodium diclofenac also resulted in a

View Article Online
DOI: 10.1039/D5QI00611F

significant (27.5-fold, $p < 0.05$, n = 18) reduction in potency compared to **4** (Figure S26, Table S5). Taken together, the control cytotoxicity studies imply that the anti-breast CSC potency of **4** is due to the preformed complex rather than any of its individual components or mixtures of its individual components. As a measure of therapeutic potential, the cytotoxicity of **4** towards a panel of non-cancerous cell lines; HEK 293 (embryonic kidney), MCF10A (epithelial breast), and BEAS-2B (bronchial epithelium) was determined (Figure S27). The nickel(II) complex **4** was significantly ($p < 0.05$, n = 18) less potent toward HEK 293 (IC_{50} = 0.30 ± 0.05 μM, 19-fold), MCF10A (IC_{50} = 0.15 ± 0.01 μM, 9-fold), and BEAS-2B (IC_{50} = 0.83 ± 0.03 μM, 52-fold) cells than HMLER-shEcad cells, therefore **4** has the potential to potently kill breast CSC-enriched cells over non-cancerous cells derived from various tissue types.

Table 1. IC_{50} values of nickel(II)-diclofenac complexes **1-4**, cisplatin, carboplatin, 5-fluorouracil, capecitabine, and salinomycin against HMLER cells, HMLER-shEcad cells, and HMLER-shEcad mammospheres. [a] Determined after 72 h incubation (mean of three independent experiments ± SD). [b] Determined after 5 days incubation (mean of three independent experiments ± SD). [c] Reported in references 43-46 and 48. n.d. not determined.

Compound	HMLER IC_{50} [μM] [a]	HMLER-shEcad IC_{50} [μM] [a]	Mammosphere IC_{50} [μM] [b]
1	7.37 ± 0.42	11.45 ± 2.46	n.d.
2	5.26 ± 0.29	14.76 ± 2.68	n.d.
3	1.17 ± 0.13	2.51 ± 0.26	79.55 ± 1.77
4	0.11 ± 0.02	0.016 ± 0.001	15.27 ± 1.62
carboplatin [c]	67.31 ± 2.80	72.39 ± 7.99	18.06 ± 0.40
cisplatin [c]	2.57 ± 0.02	5.65 ± 0.30	13.50 ± 2.34
5-fluorouracil [c]	41.05 ± 5.30	49.10 ± 5.94	15.00 ± 1.01
capecitabine [c]	> 100	> 100	> 133
salinomycin [c]	11.43 ± 0.42	4.23 ± 0.35	18.50 ± 1.50

Mammospheres are three-dimensional collections of breast CSCs that are more representative of solid tumours than monolayer cultures and provide a reliable readout of translational potential.[47] The treatment of single cell suspensions of HMLER-shEcad cells with **4** (0.13 μM) markedly reduced the number and size of mammospheres formed after 5 days incubation (Figures 2A and S28). Under the same conditions, dosage with **3** appreciably reduced the size of mammopsheres formed but not the number of mammospheres formed (Figures 2A and S28). The inhibitory effect of **4** was comparable to treatment with clinically approved breast cancer metallodrugs (cisplatin and carboplatin) and noticeably less than salinomycin under identical incubation conditions (Figures 2A and S26). The effect of **3** and **4** on mammosphere viability was determined using the colorimetric resazurin-based reagent, TOX8. Both nickel(II) complexes displayed micromolar IC_{50} values, however **4** was 5.2-fold more potent than **3**. Further, the mammosphere potency of **4** was comparable to cisplatin, carboplatin, and salinomycin (Figure S29, Table 1).[46, 48] Using a cell live (calcein AM) and cell death (propidium iodide) staining experiment, the effect of **4** on MDA-MB-231 mammospheres was evaluated. The red:green fluorescence ratio increased upon incubation with **4**. Mammosphere structural disintegration with significant loss of intercellular cohesion was also observed (Figure 2B). Taken together the mammosphere studies show that **4** is capable of multicellular spheroid penetration and cytotoxicity in three-dimensional breast cancer cultures.

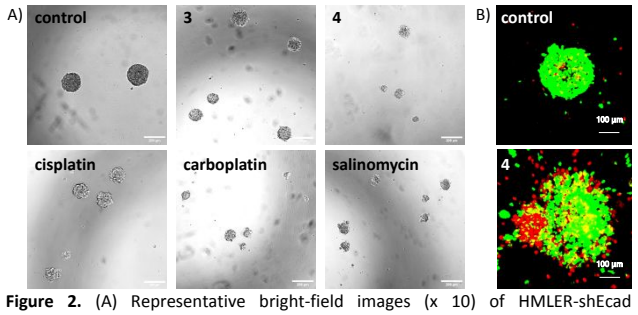

Figure 2. (A) Representative bright-field images (x 10) of HMLER-shEcad mammospheres in the absence and presence of **3**, **4**, cisplatin, carboplatin or salinomycin (0.13 μM for 5 days). Scale bar = 200 μm. (B) Representative confocal laser scanning microscopy images of MDA-MB-231 mammospheres in the absence and presence of **4** (0.5 μM for 3 days). Scale bar = 100 μm.

Induction of necroptosis in breast cancer stem cells

The mode of breast CSC death induced by **4** was investigated. Co-incubation of **4** with necroptosis pathway modulators, necrostatin-1 (RIP1 inhibitor, 20 μM)[49] or dabrafenib (RIP3 inhibitor, 10 μM),[50] significantly decreased (up to 28-fold, $p < 0.05$, n = 18) the cytotoxicity of **4** against HMLER-shEcad cells (Figure 3A, Table S6), indicating necrosome-mediated necroptosis as the mode of cell death. Complementary immunoblotting studies showed that the expression of the necrosome components RIP1, RIP3, and MLKL remained largely unaltered in HMLER-shEcad cells treated with increasing concentrations of **4** (10-50 nM for 72 h) (Figure S30). This suggests that **4**-induced necroptosis is dependent on the formation of the necrosome complex (association of RIP1, RIP3, and MLKL) and not on the perturbation of the expression of its individual protein kinase components. During necroptosis, MLKL homo-oligomers can migrate from the cytoplasm to the cell membrane and induce ion

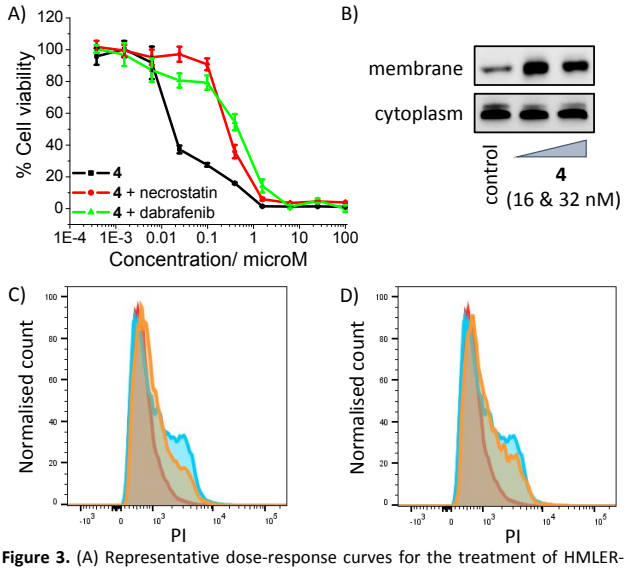

Figure 3. (A) Representative dose-response curves for the treatment of HMLER-shEcad cells with **4** after 72 h incubation in the presence and absence of nectrostatin-1 (20 μM) or dabrafenib (10 μM). (B) Immunoblotting analysis of MLKL expression in the membrane and cytosol fractions of HMLER-shEcad cells treated with **4** (16 and 32 nM for 24 h). Uncropped images of the blots are provided in the SI. (C & D) Representative histograms displaying the fluorescence emitted by PI stained HMLER-shEcad cells (red), and HMLER-shEcad cells treated with **4** (3 μM) for 24 h (blue), or **4** (3 μM) with necrostatin-1 (20 μM) or dabrafenib (10 μM) for 24 h (orange).

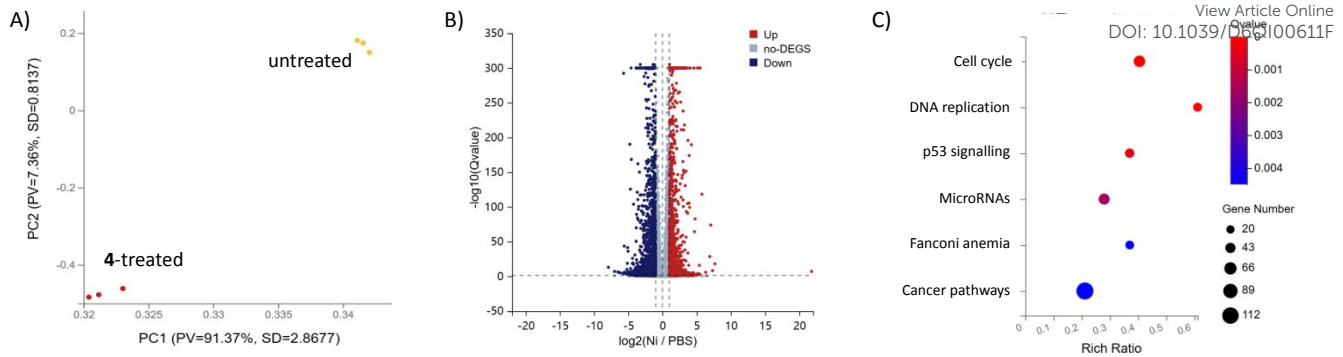

Figure 4. (A) Principal component analysis (PCA) of gene expression profiles, indicating separation between untreated 4T1 cells and **4**-treated 4T1 cells (5 μM for 12 h). (B) Volcano plot of differentially expressed genes in untreated and **4**-treated 4T1 cells (5 μM for 12 h). (C) KEGG enrichment analysis of differentially expressed genes in 4T1 cells after **4** treatment (5 μM for 12 h).

flux, leading to plasma membrane permeabilisation.[14, 51] Immunoblotting analysis of the isolated membrane and cytosol fractions of HMLER-shEcad cells treated with **4** (16 and 32 nM for 24 h) indicated a clear increase in MLKL on the membrane and a concurrent decrease in the cytosol (Figure 3B). To determine if **4** induces plasma membrane permeabilisation, propidium iodide (PI) staining studies were undertaken using flow cytometry. PI cannot penetrate or stain healthy cells, however can enter and stain cells with compromised cell membrane structures. HMLER-shEcad cells treated with **4** (3 μM for 24 h) displayed increased PI uptake relative to untreated cells, suggestive of cell membrane permeabilisation (Figure 3C-D). When **4** (3 μM for 24 h) was co-treated with necrostatin-1 (20 μM) or dabrafenib (10 μM), PI uptake was attenuated (Figure 3C-D), implying that **4**-induced plasma membrane permeabilisation is associated to necrosome formation and potentially related to MLKL migration. Although the plasma membrane is compromised during necroptosis, the nuclear membrane is typically preserved.[52] Bright-field microscopy studies of HMLER-shEcad cells treated with **4** (4 × IC_{50} value for 24 h) showed that some cells displayed cell membrane disruption while their nuclear membrane was preserved (Figure S31), consistent with necroptotic cell death. The morphological features induced by **4** in HMLER-shEcad cells disappeared in the presence of necrostatin-1 (20 μM) and dabrafenib (10 μM), implying that they were related to necrosome formation (Figure S31).

Cellular uptake and fractionation studies were conducted to determine the ability of **4** to enter breast CSCs. Specifically, HMLER-shEcad cells were incubated with **4** (0.25 μM for 24 h) and the internalised nickel content was determined by inductively coupled plasma mass spectrometry (ICP-MS) (Figure S32). The nickel(II) complex **4** was readily taken up by breast CSCs, with whole cell uptake detected as 7.3 ± 0.3 ng of Ni/ million cells. Fractionation studies indicated that a large proportion of internalised **4** was detected in the cytoplasm (81%), as opposed to the nucleus or membrane, suggesting that **4**-mediated breast CSC toxicity is likely to be related to interactions with cytoplasmic biomolecules, consistent with the induction of necroptosis.

A common hallmark of necroptosis is the hyperactivation of PARP-1, which can result from DNA damage and lead to the depletion of ATP and NAD levels.[53, 54] The cytotoxicity of **4** towards HMLER-shEcad cells significantly decreased ($p < 0.05$, n = 18) in the presence of well-known PARP-1 inhibitors, veliparib (10 μM, IC_{50} = 0.20 ± 0.006 μM, 12.5-fold)[55] and 4-amino-1,8-naphthalimide (10 μM, IC_{50} = 0.18 ± 0.005 μM, 11-fold)[56] (Figure S33, Table S6), suggesting that hyperactivation of PARP-1 was part of necroptosis mechanism evoked by **4**. Immunoblotting studies revealed that HMLER-shEcad cells treated with **4** (1-3 μM for 72 h) expressed higher levels of phosphorylated H2AX (γH2AX) and CHK2 than untreated cells, indicative of genomic DNA damage (Figure S34).[57, 58] Transcriptomic RNA sequencing (RNA-seq) analysis of mouse mammary carcinoma 4T1 cells treated with **4** (5 μM for 12 h) revealed significant changes in intracellular signaling pathways (528 uniquely expressed genes) compared to untreated cells (Figures 4A-B). Gene Ontology (GO) enrichment analysis showed that **4**-treated 4T1 cells affected kinetochore and chromosome genes in the cellular component (Figure S35A), the processes of cell cycle, cell division, and DNA replication in the biological process (Figure S35B), single stranded DNA-dependent ATP-dependent binding in the molecular function (Figure S35C). Kyoto Encyclopedia of Genes and Genomes (KEGG) analysis indicates that cell cycle and DNA replication are affected by **4** (Figure 4C). According to cell cycle analysis, **4** (75-150 nM for 72 h) stalls HMLER-shEcad cells at the G1 phase (Figure S36), consistent with the RNA-seq data. G1-phase cell cycle arrest is also allied to necroptosis.[59, 60] The amalgamation of the necrosome complex can lead to downstream reactive oxygen species (ROS) generation.[61, 62] To determine if **4**-induced necroptosis leads to intracellular ROS elevation, 6-carboxy-2',7'-dichlorodihydrofluorescein diacetate (DCFH-DA) was used. HMLER-shEcad cells dosed with **4** (32 nM) displayed a time-dependent increase in ROS levels compared to untreated cells over the course of 24 h (Figure S37). This suggests that **4** is unlikely to intrinsically generate ROS and the time-dependent ROS level elevation observed is a downstream outcome (possibly through necrosome formation). Given this implication, **4** is not expected to induce DNA damage via inherent ROS production but possibly via necroptosis-associated hyperactivation of PARP-1. To determine if **4**-induced ROS elevation results in breast CSC death, independent cell viability studies were carried out in the presence of *N*-acetylcysteine (2.5 mM), a ROS scavenger. In the presence of *N*-acetylcysteine the potency of **4** towards HMLER-shEcad cells decreased significantly (IC_{50} = 0.18 ± 0.004 μM, 11-fold, $p < 0.05$, n = 18) (Figure S38, Table S6), suggesting that **4**-induced breast CSC death is related to ROS elevation.

DOI: 10.1039/D6QI00611F

Modulation of cycloogenase-2 expression and impact on cell death

Given that **4** comprises of two diclofenac moieties and is designed to modulate COX-2 levels, flow cytometric studies were conducted to determine the impact of **4** on COX-2 expression and thus the iDAMP axis. HMLER-shEcad cells pre-treated with lipopolysaccharide (LPS) (2.5 μM for 24 h), to increase basal COX-2 levels, were treated with **4** (IC_{50} value and 2 × IC_{50} value for 48 h) and the COX-2 expression was determined. COX-2 expression decreased significantly upon treatment with **4** (Figure S39). Diclofenac-treated (20 μM for 48 h) HMLER-shEcad cells also exhibit noticeably lower levels of COX-2 compared to untreated cells (Figure S40A). HMLER-shEcad cells treated with [Ni^{II}(4,7-diphenyl-1,10-phenanthroline)Cl_2] (2 × IC_{50} value for 48 h) did not display a marked change in COX-2 expression compared to untreated cells (Figure S40B). This suggests that **4**-induced downregulation of COX-2 in breast CSCs is associated to the diclofenac moieties in **4**. To determine if **4** induces COX-2-dependent breast CSC death, cytotoxicity studies were performed with HMLER-shEcad cells co-treated with prostaglandin E2 (20 μM). The potency of **4** towards HMLER-shEcad cells decreased significantly (IC_{50} = 0.34 ± 0.05 μM, 21-fold, $p < 0.05$, n = 18) under these conditions (Figure S41). Overall, the flow cytometric and cytotoxicity studies suggest that the mechanism of action of **4** could be related to COX-2 downregulation and iDAMP perturbation.

Immunogenic phenotype and phagocytosis of breast cancer stem cells

Given the ability of **4** to downregulate COX-2 and induce necroptosis in breast CSCs, we investigated whether **4** can induce DAMP release from breast CSCs. Four major DAMPs allied to ICD, adenosine triphosphate (ATP), nuclear high mobility group box 1 (HMGB-1), calreticulin (CRT), and phosphatidylserine (PS) were monitored.[30] HMLER-shEcad cells treated with **4** (3-5 μM for 24 h) released ATP in a dose-dependent manner (up to 6.6-fold more than untreated cells) according to an established luciferase-based assay (Figure 5A). Dosage with cisplatin (50-100 μM for 24 h) also induced significant ATP release (up to 6.4-fold more than untreated cells) (Figure 5A). Immunoblotting studies showed that HMLER-shEcad cells treated with **4** (1-5 μM for 72 h) displayed markedly lower or undetectable amounts of HMGB-1 relative to untreated cells, indicative of HMGB-1 expulsion (Figure 5B). According to flow cytometric studies, HMLER-shEcad cells dosed with **4** (3 μM for 24 h or 72 h) did not display markedly higher levels of CRT on their cell membrane compared to untreated cells (Figure S42). This phenomenon is consistent with immunogenic hallmarks resulting from cells that have undergone necroptosis.[63, 64] In fact, CRT exposure is not a prerequisite for the phagocytosis of necroptotic cells by immune cells.[63, 64] As expected, HMLER-shEcad cells dosed with cisplatin (150 μM for 24 h or 72 h) and thapsigargin (7 μM for 24 h or 72 h) displayed an increase in CRT on their cell membrane (Figure S43). Although CRT exposure is not synonymous with necroptotic cells, PS externalisation is a common feature and functions as a 'find me' and

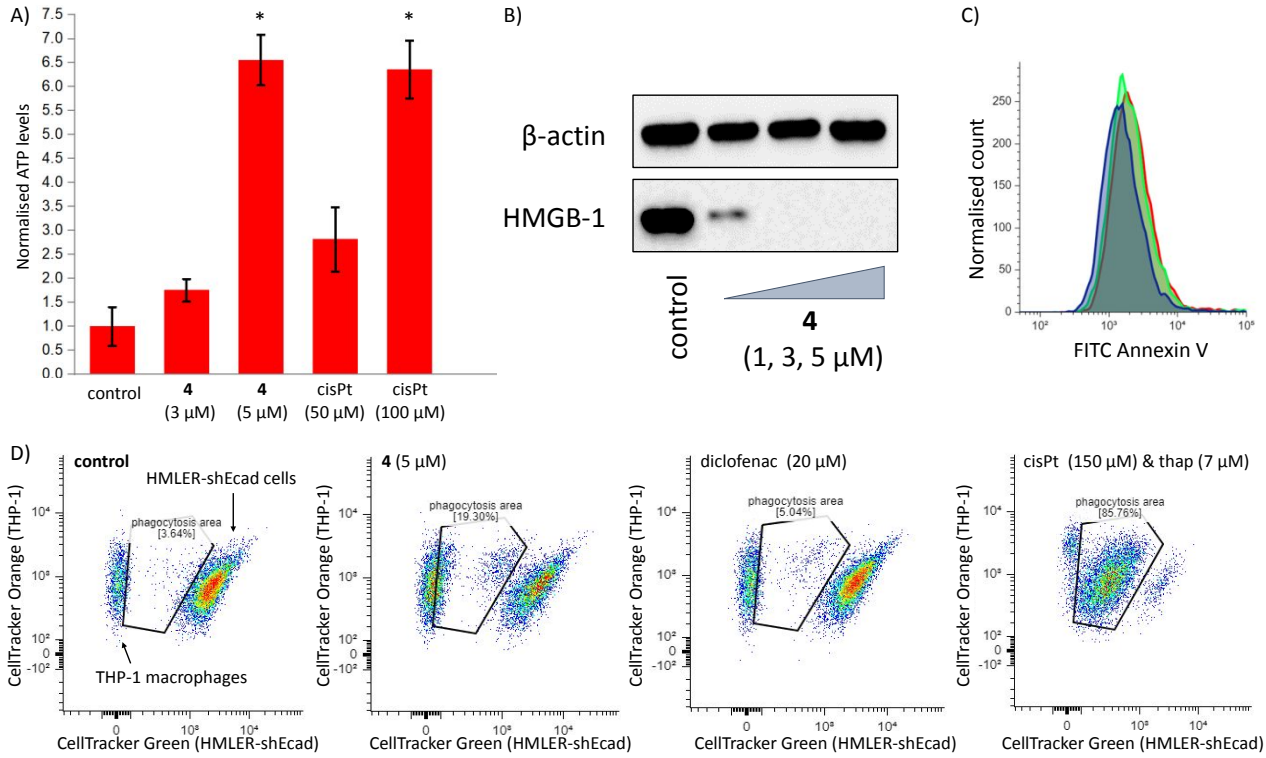

Figure 5. (A) Normalised extracellular ATP released from HMLER-shEcad cells untreated and treated with **4** (3 μM or 5 μM) or cisplatin (50 μM or 100 μM) for 24 h. The data is represented as the mean ± SD (* $p < 0.01$, Student's t-test). (B) Immunoblotting analysis of high mobility group box 1 (HMGB-1). Protein expression in HMLER-shEcad cells following treatment with **4** (1-5 μM) for 72 h. Uncropped images of the blots are provided in the SI. (C) Representative histograms displaying the green fluorescence emitted by FITC Annexin V-stained HMLER-shEcad cells untreated (blue, median: 1556.9 ± 78.0), and treated with **4** (64 nM) (green, median: 1948.4 ± 97.4) or **4** (128 nM) (red, median: 2176.2 ± 43.5) for 72 h. (D) Representative two-dimensional scatter plots of CellTracker Green-stained HMLER-shEcad cells untreated and treated with **4** (5 μM) or diclofenac (20 μM) or cisplatin (150 μM) and thapsigargin (7 μM) for 24 h and then co-cultured with CellTracker Orange-stained THP-1 macrophages for 2 h.

View Article Online
DOI: 10.1039/D6QI00641F

'eat me' signal for immune cells.[16] HMLER-shEcad cells treated with **4** (64 and 128 nM for 24 h) displayed a distinct increase in PS on their cell membrane (Figure 5C) suggesting that **4**-induced breast CSC death may lead to an immunogenic effect through PS exposure. Overall, the DAMP detection studies suggest that **4** is capable of evoking an immunogenic phenotype in breast CSCs that does not display all the hallmarks of ICD.

We next investigated the ability of HMLER-shEcad cells treated with **4** to be phagocytosed by macrophages. HMLER-shEcad cells pre-stained with CellTracker Green were treated with **4** (5 μM for 24 h) and then incubated with macrophages pre-stained with CellTracker Orange for 2 h. The population of double-stained macrophages and engulfed HMLER-shEcad cells is indicated in the two-dimensional scatter plots shown in Figure 5D. The nickel(II) complex **4** (5 μM for 24 h) was able to significantly enhance engulfment of HMLER-shEcad cells by macrophages (5.3-fold increase compared to untreated cells, Figure 5D). HMLER-shEcad cells treated with diclofenac (20 μM for 24 h) did not induce significant phagocytosis by macrophages (Figure 5D). This implies that the necroptosis-inducing nickel(II)-phenanthroline moiety in **4** is vital for prompting phagocytosis of breast CSCs by macrophages. The addition of cisplatin (150 μM for 24 h) and thapsigargin (7 μM for 24 h) to HMLER-shEcad cells resulted in a significant increase in the population of double-stained macrophages (23.5-fold increase compared to untreated cells, Figure 5D) indicative of phagocytosis. Overall, the phagocytosis assay shows that **4** is able to kill breast CSCs in a manner that promotes engulfment by macrophages.

Immunotherapeutic efficacy in a murine breast cancer model

To ensure intact delivery of **4** to breast tumour sites *in vivo*, **4** was encapsulated into polymeric nanoparticles. We used the thioketal bond-containing, ROS-responsive, amphiphilic polymer, PSP to encapsulate **4** (Figure 6A). PSP was synthesized using a previously reported protocol (Scheme S1).[65] The nanoprecipitation method was employed to encapsulate **4** (5 mg/mL) into the hydrophobic core of PSP (50 mg/mL) to produce **4**-loaded PSP nanoparticles **NP-4** (Figure 6A). The concentration of **4** in **NP-4** was determined by atomic absorption spectrometry (AAS). The average nanoparticle size of **NP-4** measured by dynamic light scattering (DLS) was 133.3 nm and the polydispersity was 0.05 (Figure 6B-C). The morphology of **NP-4** was probed by transmission electron microscopy (TEM). As depicted in Figure 6D, **NP-4** had spherical morphology with a uniform size distribution. Given the presence of ROS-responsive thioketal bonds in PSP, the release profile of **NP-4** was studied in the presence of H_2O_2 over the course of 48 h. After 48 h incubation, **NP-4** was able to release 2.5-fold more **4** in the presence of H_2O_2 (10 mM) compared to the PBS control group (Figure 6E). This shows that **NP-4** can potentially release its payload more effectively in ROS-enriched areas of the body, such as the cancer microenvironment or inside cancer cells.[66]

The distribution of **NP-4** and **4** in BALB/c mice bearing 4T1 breast tumours was determined by intravenous administration of **NP-4** (5 mg Ni kg^{-1}) or **4** (5 mg Ni kg^{-1}), organ harvesting after 3 days, and analysis of the nickel content in each tissue by AAS (n = 4 mice) (Figure S44). **NP-4** was found to primarily accumulate in the kidneys and spleen, whereas **4** accumulated predominantly in the kidneys and lungs (Figure 7A-B). Comparative analysis of nickel levels in the tumour showed that **NP-4** exhibited 1.8-fold higher tumour accumulation than **4** (Figure 7C). This suggests that the encapsulation of **4** by PSP nanoparticles enhances tumour accumulation (possibly via the enhanced permeability and retention effect).

Next, the ability of **NP-4** to modulate tumour growth in 4T1 breast cancer-bearing mice was determined. Survival analysis and maximum tolerated dose studies (n = 4 mice) were conducted with four doses to determine the administration dose for the tumour growth inhibition studies (Figure S45). The study showed that the body weight of the mice was relatively stable when dosed with 0.5 mg Ni kg^{-1} or 1.5 mg Ni kg^{-1} of **NP-4** over a 10 day period. When the dose was increased to 2.5 mg Ni kg^{-1} of **NP-4**, two mice in this treatment group experienced approximately 20% body weight loss. At the higher dose of 5 mg Ni kg^{-1} of **NP-4**, all mice showed around 20% body weight reduction. Among them, two mice died on the 6th day, and the other two died on the 8th day. Based on these results 1.5 mg Ni kg^{-1} of **NP-4** was selected as the administration dose for

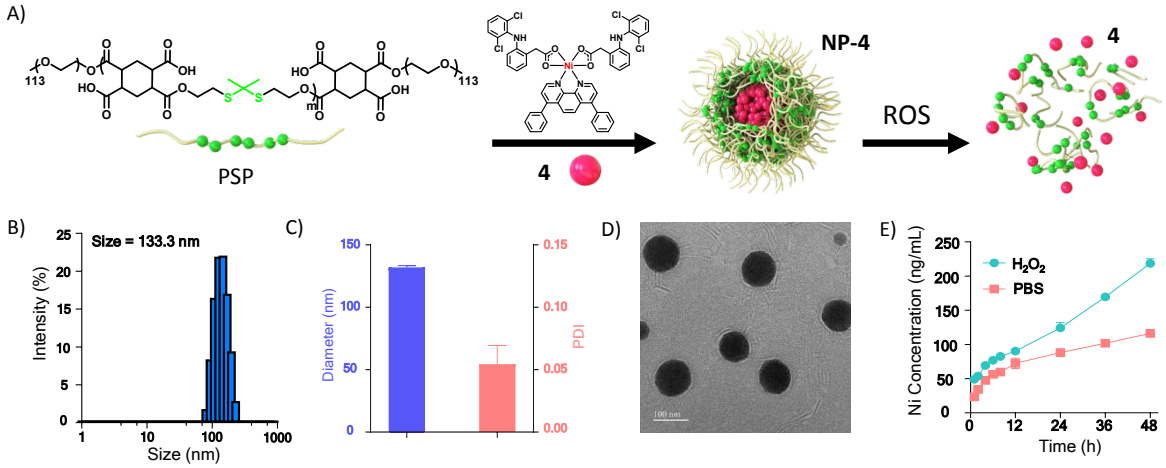

Figure 6. (A) Schematic showing the encapsulation of **4** into PSP polymeric nanoparticles (**NP-4**) and the ROS-triggered release of **4** from **NP-4**. (B and C) The average nanoparticle size and PDI of **NP-4** determined by DLS. (D) Representative TEM images of **NP-4**. Scale bar = 100 μm. (E) Representative nickel release profiles of **NP-4** in PBS alone and in PBS with H_2O_2 (10 mM) at 37 °C over the course of 48 h.

View Article Online
DOI: 10.1039/D5QI00611F

the tumour growth inhibition studies. Once BALB/c mice inoculated with 4T1 cells displayed tumours with a volume of about 50 mm^3, the nanoparticle formulation **NP-4** (1.5 mg Ni kg^{-1}) was administered intravenously every 2 days for 8 days (n = 4 mice) and the tumour size was monitored every 2 days for 12 days (Figure 7D). Negative and positive control groups (n = 4 mice) were treated with the vehicle (PBS), doxorubicin (1.5 mg kg^{-1}, clinically used chemotherapeutic agent with immunogenic properties *in vivo*[67, 68]) or oxaliplatin (1.5 mg Pt kg^{-1}, clinically used anticancer metallodrug with ICD-inducing properties *in vivo*[69, 70]). As depicted in Figures 7E and S46, tumour growth was significantly inhibited in the **NP-4**-treated group with respect to the control group (47% smaller tumours after 12 days). Additionally, the tumour growth inhibitory profile of the **NP-4**-treated group was significantly (p < 0.01) stronger than the doxorubicin- and oxaliplatin-treated groups (Figures 7E and S46). In all cases, treated mice maintained their body weight relative to the control group throughout the course of the study (Figure S47).

Given the ability of **4** to induce an immunogenic phenotype in breast CSCs *in vitro*, the immunotherapeutic efficacy of **NP-4** was investigated in immunocompetent 4T1 breast cancer-bearing BALB/c mice. Immunogenic agents promote the recruitment and infiltration of immune cells (mature dendritic cells and T-cells) into the lymph nodes and tumours.[71] 4T1 tumour-bearing mice were subject to intravenous administration of **NP-4** (1.5 mg Ni kg^{-1}) or doxorubicin (1.5 mg kg^{-1}) or oxaliplatin (1.5 mg Pt kg^{-1}) or the vehicle (PBS) every 2 days for 8 days (n = 3 mice) and after 12 days the lymph nodes and tumours were extracted and analysed by flow cytometry using relevant immune cell markers (Figure S48). Analysis of tumour-draining lymph nodes revealed that mice treated with **NP-4** exhibited significantly higher levels of $CD8^+$ $CD69^+$ T-cells (17.0%) than to those treated with doxorubicin (13.9%), oxaliplatin (15.5%) or the vehicle (11.2%) (Figure S49). Furthermore, the proportion of $CD80^+$ $CD86^+$ mature dendritic cells in the tumour-draining lymph nodes of mice treated with **NP-4** (36.3%) was approximately twice that of mice treated with the vehicle (17.6%) and markedly more than those treated with doxorubicin (28.2%) or oxaliplatin (28.6%) (Figure S50). Since mature dendritic cells can activate T lymphocytes and trigger an adaptive immune response,[72] the proportions of tumour infiltrating $CD4^+$ and $CD8^+$ T-cells were examined. The percentage of $CD8^+$ T-cells in tumours of mice treated with **NP-4** (33.1%) was significantly higher than in tumours of mice treated with the vehicle (22.5%) and markedly more than those treated with doxorubicin (26.6%) or oxaliplatin (29.4%) (Figure S51). An increase in the percentage of $CD4^+$ T-cells in tumours of mice treated with **NP-4** (55.6%) compared to the control group (47.5%) was also observed (Figure S46). The proportion of tumour infiltrating $CD8^+$ T-cells was also gauged by histological studies (Figure S51). Noticeably more $CD8^+$ T-cells (cells stained red) were detected in tumour samples taken from mice treated with **NP-4** compared to those taken from mice treated with oxaliplatin or the vehicle (Figure S52). Overall, the *in vivo* results support proof-of-concept that intratumorally delivery of the nickel(II) complex **4** can be achieved by PSP nanoparticles and that the formulation can induce an immunogenic effect. It is acknowledged that no functional assessment of anti-tumour immunity was performed.

Conclusions

In summary we report the synthesis, characterisation, and anti-breast CSC properties of a series of nickel(II)-polypyridyl complexes **1**-**4** containing two diclofenac moieties. Time course UV-vis spectroscopy and mass spectrometry studies indicated that **1**-**4** are stable in cell culture conditions and in the presence of cellular reductants (ascorbic acid and glutathione). HPLC analysis provided

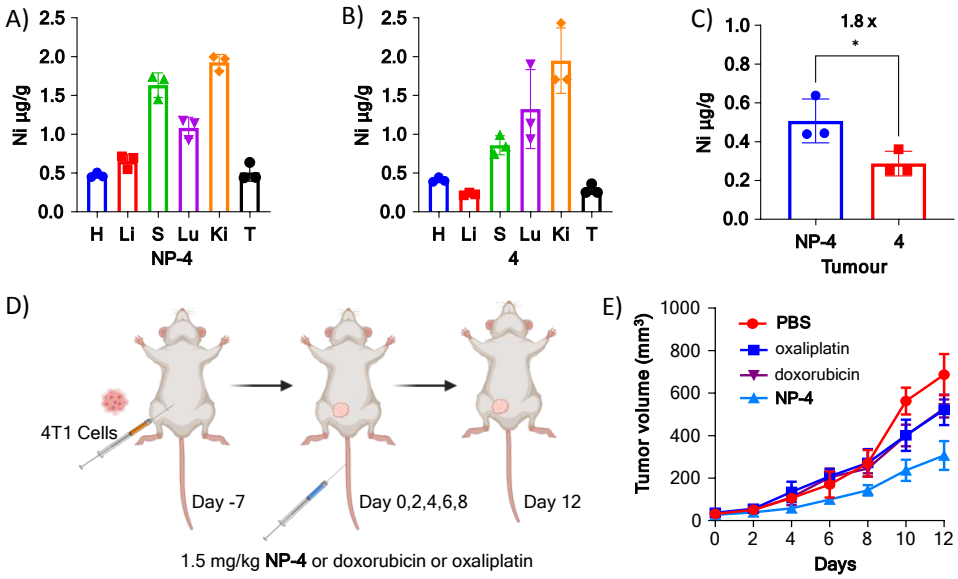

Figure 7. Biodistribution of nickel in 4T1 tumour-bearing mice following treatment with (A) **NP-4** (5 mg Ni kg^{-1}) or (B) **4** (5 mg Ni kg^{-1}) (n = 4 mice). H: heart, Li: liver, S: spleen, Lu: lungs, Ki: kidney, and T: tumour. (C) Differential tumor accumulation of **NP-4** and **4**. (D) Schematic of the experimental design for determining the tumour growth inhibition profiles. (E) Averaged tumor growth inhibition curves of 4T1 tumour-bearing mice (n = 4 mice), following intravenous administration of the vehicle (PBS) or doxorubicin (1.5 mg kg^{-1}) or oxaliplatin (1.5 mg Pt kg^{-1}) or **NP-4** (1.5 mg Ni kg^{-1}).

further evidence that **4** was stable in cell culture media, and UV-vis spectroscopy and ICP-MS studies showed that **4** was stable in human plasma and resistant to nickel leaching. Cytotoxicity studies showed that **4** displayed the highest potency towards breast CSCs within the series and was an astonishing 264-fold and 353-fold more potent than salinomycin and cisplatin, respectively. Mechanistic studies revealed that **4** is able to induce necroptosis in breast CSCs by necrosome-mediated and MLKL migration-associated plasma membrane permeabilisation. Detailed cell-based studies also showed that intracellular ROS elevation and PARP-1 hyperactivation (possibly due to genomic DNA damage) are part of the necroptosis mechanism evoked by **4**. Furthermore, **4** is able to reduce COX-2 expression in breast CSCs. The potency of **4** toward breast CSCs was attenuated in the presence of prostaglandin E2 (an iDAMP), implying that the mechanism of action of **4** could be related to COX-2 downregulation. DAMP detection studies indicated that **4** is able to promote extracellular release of ATP and HMGB-1 and lead to PS (but not CRT) exposure on the membrane, consistent with a necroptosis-associated and iDAMP-modulating immunogenic phenotype (which is not fully consistent with ICD). Phagocytosis studies showed that breast CSCs treated with **4** were efficiently engulfed by macrophages, highlighting the promising immunogenic potential of **4**. *In vivo* studies with immunocompetent 4T1 breast cancer-bearing mice, showed that upon encapsulation of **4** into polymeric nanoparticles **NP-4** and intravenous administration, tumour progression was significantly inhibited and a robust immune response was evoked. Taken together, the *in vivo* studies suggest that **4** is an efficacious immunotherapeutic agent with very promising translatable scope. We believe this study provides fresh impetus to explore the biological activity of nickel coordination complexes. The results also pave the way for the development of other metal-NSAID complexes as necroptosis-inducing, iDAMP-modulating immunotherapeutics for CSC-directed treatment.

Author contributions

Conceptualization, F.O., H.X., and K.S.; methodology, A.G.B., M.C., X.F., K.S., F.O., H.X., and K.S.; validation, A.G.B., M.C., X.F., K.S., F.O., H.X., and K.S.; formal analysis, A.G.B., M.C., X.F., K.S., F.O., H.X., and K.S.; investigation, A.G.B., M.C., X.F., K.S., F.O., H.X., and K.S.; writing—original draft preparation, A.G.B., M.C., H.X., and K.S.; writing—review and editing, A.G.B., M.C., X.F., K.S., F.O., H.X., and K.S.; supervision, F.O., H.X., and K.S.; project administration, F.O., H.X., and K.S.; funding acquisition, F.O., H.X., and K.S. All authors have read and agreed to the published version of the manuscript.

Conflicts of interest

There are no conflicts to declare.

Data availability

The data supporting this article have been included as part of the Supplementary Information. Crystallographic data for **2** has been deposited at the CCDC under 2483096 and can be obtained from www.ccdc.cam.ac.uk/data_request/cif.

Acknowledgements

K.S. and F.O. are supported by EPSRC New Investigator Awards (EP/S005544/1 and EP/W00691X/1). H.X. thanks the National Natural Science Foundation of China (U24A202246) and the International Partnership Program of Chinese Academy of Sciences for Future Network (027GJHZ2023144FN) for funding. X.F. is supported by a Chinese Scholarship Council PhD studentship. The Advanced Imaging Facility (RRID:SCR_020967) at the University of Leicester is also thanked. XRD crystallography at the University of Leicester is supported by an EPSRC Core Equipment Award (EP/V034766/1). NMR Spectroscopy at the University of Leicester is supported by an EPSRC Strategic Equipment Award (EP/W02151X/1).

Notes and references

1. N. El-Sayes, A. Vito and K. Mossman, Tumor Heterogeneity: A Great Barrier in the Age of Cancer Immunotherapy, *Cancers*, 2021, **13**.
2. X. Chu, W. Tian, J. Ning, G. Xiao, Y. Zhou, Z. Wang, Z. Zhai, G. Tanzhu, J. Yang and R. Zhou, Cancer stem cells: advances in knowledge and implications for cancer therapy, *Sig. Transduct. Target. Ther.*, 2024, **9**, 170.
3. W. Chen, J. Dong, J. Haiech, M. C. Kilhoffer and M. Zeniou, Cancer Stem Cell Quiescence and Plasticity as Major Challenges in Cancer Therapy, *Stem Cells Int.*, 2016, **2016**, 1740936.
4. L. N. Abdullah and E. K. Chow, Mechanisms of chemoresistance in cancer stem cells, *Clin. Transl. Med.*, 2013, **2**, 3.
5. M. Dean, T. Fojo and S. Bates, Tumour stem cells and drug resistance, *Nat. Rev. Cancer*, 2005, **5**, 275-284.
6. K. Rycaj and D. G. Tang, Cancer stem cells and radioresistance, *Int. J. Radiat. Biol.*, 2014, **90**, 615-621.
7. V. D'Andrea, S. Guarino, F. M. Di Matteo, M. Maugeri Sacca and R. De Maria, Cancer stem cells in surgery, *G Chir.*, 2014, **35**, 257-259.
8. J. Lathia, H. Liu and D. Matei, The Clinical Impact of Cancer Stem Cells, *Oncologist*, 2020, **25**, 123-131.
9. Y. Shiozawa, B. Nie, K. J. Pienta, T. M. Morgan and R. S. Taichman, Cancer stem cells and their role in metastasis, *Pharmacol. Ther.*, 2013, **138**, 285-293.
10. N. Badrinath and S. Y. Yoo, Recent Advances in Cancer Stem Cell-Targeted Immunotherapy, *Cancers*, 2019, **11**.
11. U. Fischer and K. Schulze-Osthoff, Apoptosis-based therapies and drug targets, *Cell Death Differ.*, 2005, **12 Suppl 1**, 942-961.
12. P. Vandenabeele, L. Galluzzi, T. Vanden Berghe and G. Kroemer, Molecular mechanisms of necroptosis: an ordered cellular explosion, *Nat. Rev. Mol. Cell Biol.*, 2010, **11**, 700-714.
13. J. Li, T. McQuade, A. B. Siemer, J. Napetschnig, K. Moriwaki, Y. S. Hsiao, E. Damko, D. Moquin, T. Walz, A. McDermott, F. K. Chan and H. Wu, The RIP1/RIP3 necrosome forms a functional amyloid signaling complex required for programmed necrosis, *Cell*, 2012, **150**, 339-350.
14. Z. Cai, S. Jitkaew, J. Zhao, H. C. Chiang, S. Choksi, J. Liu, Y. Ward, L. G. Wu and Z. G. Liu, Plasma membrane translocation of trimerized MLKL protein is required for TNF-induced necroptosis, *Nat. Cell Biol.*, 2014, **16**, 55-65.
15. A. G. Snyder, N. W. Hubbard, M. N. Messmer, S. B. Kofman, C. E. Hagan, S. L. Orozco, K. Chiang, B. P. Daniels, D. Baker and A. Oberst, Intratumoral activation of the necroptotic pathway

components RIPK1 and RIPK3 potentiates antitumor immunity, *Sci. Immunol.*, 2019, **4**.
16. J. Sprooten, P. De Wijngaert, I. Vanmeerbeerk, S. Martin, P. Vangheluwe, S. Schlenner, D. V. Krysko, J. B. Parys, G. Bultynck, P. Vandenabeele and A. D. Garg, Necroptosis in Immuno-Oncology and Cancer Immunotherapy, *Cells*, 2020, **9**.
17. M. Pasparakis and P. Vandenabeele, Necroptosis and its role in inflammation, *Nature*, 2015, **517**, 311-320.
18. V. Novohradsky, L. Markova, H. Kostrhunova, Z. Trávníček, V. Brabec and J. Kasparkova, An anticancer Os(II) bathophenanthroline complex as a human breast cancer stem cell-selective, mammosphere potent agent that kills cells by necroptosis, *Sci. Rep.*, 2019, **9**.
19. M. Flamme, P. B. Cressey, C. Lu, P. M. Bruno, A. Eskandari, M. T. Hemann, G. Hogarth and K. Suntharalingam, Induction of Necroptosis in Cancer Stem Cells using a Nickel(II)-Dithiocarbamate Phenanthroline Complex, *Chem. Eur. J.*, 2017, **23**, 9674-9682.
20. A. Eskandari, M. Flamme, Z. Xiao and K. Suntharalingam, The Bulk Osteosarcoma and Osteosarcoma Stem Cell Activity of a Necroptosis-Inducing Nickel(II)-Phenanthroline Complex, *ChemBioChem*, 2020, **21**, 2854-2860.
21. C. J. Feld, A. Johnson, Z. Xiao and K. Suntharalingam, Breast Cancer Stem Cell Potency of Nickel(II)-Polypyridyl Complexes Containing Non-steroidal Anti-inflammatory Drugs, *Chem. Eur. J.*, 2020, **26**, 14011-14017.
22. G. Passeri, J. Northcote-Smith, R. Perera, N. Gubic and K. Suntharalingam, An Osteosarcoma Stem Cell Potent Nickel(II)-Polypyridyl Complex Containing Flufenamic Acid, *Molecules*, 2022, **27**, 3277.
23. D. Josa, P. Herrera-Ramírez, X. Feng, A. Gutiérrez, D. Aguilà, A. Grabulosa, M. Martínez, K. Suntharalingam and P. Gamez, Cyclometalated half-sandwich iridium(III) and rhodium(III) complexes as efficient agents against cancer stem-cell mammospheres, *Inorg. Chem. Front.*, 2025, **12**, 2404-2416.
24. N. Aztopal, D. Karakas, B. Cevatemre, F. Ari, C. Icsel, M. G. Daidone and E. Ulukaya, A trans-platinum(II) complex induces apoptosis in cancer stem cells of breast cancer, *Bioorg. Med. Chem.*, 2017, **25**, 269-276.
25. S. Kimani, S. Chakraborty, I. Irene, J. de la Mare, A. Edkins, A. du Toit, B. Loos, A. Blanckenberg, A. Van Niekerk, L. V. Costa-Lotufo, K. N. ArulJothi, S. Mapolie and S. Prince, The palladacycle, BTC2, exhibits anti-breast cancer and breast cancer stem cell activity, *Biochem. Pharmacol.*, 2021, **190**, 114598.
26. K. Xiong, C. Qian, Y. Yuan, L. Wei, X. Liao, L. He, T. W. Rees, Y. Chen, J. Wan, L. Ji and H. Chao, Necroptosis Induced by Ruthenium(II) Complexes as Dual Catalytic Inhibitors of Topoisomerase I/II, *Angew. Chem. Int. Ed.*, 2020, **59**, 16631-16637.
27. J. Gonçalves, J. D. Amaral, R. Capela, M. d. J. Perry, C. Braga, M. M. Gaspar, F. M. Piedade, L. Bijlsma, A. Roig, S. N. Pinto, R. Moreira, P. Florindo and C. M. P. Rodrigues, Necroptosis induced by ruthenium (II) complexes as mitochondrial disruptors, *Cell Death Discov.*, 2024, **10**, 261.
28. L. Y. Pang, E. A. Hurst and D. J. Argyle, Cyclooxygenase-2: A Role in Cancer Stem Cell Survival and Repopulation of Cancer Cells during Therapy, *Stem Cells Int.*, 2016, **2016**, 11.
29. K. Hayashi, F. Nikolos, Y. C. Lee, A. Jain, E. Tsouko, H. Gao, A. Kasabyan, H. E. Leung, A. Osipov, S. Y. Jung, A. V. Kurtova and K. S. Chan, Tipping the immunostimulatory and inhibitory DAMP balance to harness immunogenic cell death, *Nature Commun.*, 2020, **11**, 6299.
30. D. V. Krysko, A. D. Garg, A. Kaczmarek, O. Krysko, P. Agostinis and P. Vandenabeele, Immunogenic cell death and DAMPs in cancer therapy, *Nat. Rev. Cancer*, 2012, **12**, 860-875.
31. Q. Pan, Q. Li, S. Liu, N. Ning, X. Zhang, Y. Xu, A. E. Chang and M. S. Wicha, Concise Review: Targeting Cancer Stem Cells Using Immunologic Approaches, *Stem Cells*, 2015, **33**, 2085-2092.
32. V. S. Bruttel and J. Wischhusen, Cancer stem cell immunology: key to understanding tumorigenesis and tumor immune escape?, *Front. Immunol.*, 2014, **5**, 360.
33. J. Fang, O. N. Orobator, C. Olelewe, G. Passeri, K. Singh, S. G. Awuah and K. Suntharalingam, A Breast Cancer Stem Active Cobalt(III)-Cyclam Complex Containing Flufenamic Acid with Immunogenic Potential, *Angew. Chem. Int. Ed.* , 2024, **63**, e202317940.
34. R. Altman, B. Bosch, K. Brune, P. Patrignani and C. Young, Advances in NSAID development: evolution of diclofenac products using pharmaceutical technology, *Drugs*, 2015, **75**, 859-877.
35. W. Zhang, L.-M. Yang, Y. Zhao, M.-Y. Li, Y.-Q. Shi, Y. Lu, X.-S. Wang, S. He, F.-Y. Wang, K.-B. Huang and H. Liang, Stable Cyclometalated Gold(III) Complex Engaging Isoquinoline Derivative and Disulfur Ligand Elicits Necroptosis-Dependent Immunogenic Cell Death, *J. Med. Chem.*, 2026, **69**, 4932-4944.
36. D. Martinez, M. Motevalli and M. Watkinson, Is there really a diagnostically useful relationship between the carbon-oxygen stretching frequencies in metal carboxylate complexes and their coordination mode?, *Dalton Trans.*, 2010, **39**, 446-455.
37. G. B. Deacon and R. J. Phillips, Relationships between the carbon-oxygen stretching frequencies of carboxylato complexes and the type of carboxylate coordination, *Coord. Chem. Rev.*, 1980, **33**, 227-250.
38. D. Karthickram, N. Bhuvanesh and K. Sundaravel, Nickel(II) Complexes of Sterically Hindered 3N Donor Ligands as Models for Quercetin-2,4-Dioxygenase: Impact of Terminal Amine Substituent on Dioxygenolysis Reactivity, *Eur. J. Inorg. Chem.*, 2024, **27**, e202400547.
39. M. Kyropoulou, C. P. Raptopoulou, V. Psycharis and G. Psomas, Ni(II) complexes with non-steroidal anti-inflammatory drug diclofenac: Structure and interaction with DNA and albumins, *Polyhedron*, 2013, **61**, 126-136.
40. Cambridge Crystallographic Data Centre deposition number 2483096 for complex **2**.
41. P. B. Gupta, T. T. Onder, G. Jiang, K. Tao, C. Kuperwasser, R. A. Weinberg and E. S. Lander, Identification of Selective Inhibitors of Cancer Stem Cells by High-Throughput Screening, *Cell*, 2009, **138**, 645-659.
42. M. Al-Hajj, M. S. Wicha, A. Benito-Hernandez, S. J. Morrison and M. F. Clarke, Prospective identification of tumorigenic breast cancer cells, *Proc. Natl. Acad. Sci. U.S.A.*, 2003, **100**, 3983-3988.
43. J. N. Boodram, I. J. McGregor, P. M. Bruno, P. B. Cressey, M. T. Hemann and K. Suntharalingam, Breast Cancer Stem Cell Potent Copper(II)-Non-Steroidal Anti-Inflammatory Drug Complexes, *Angew. Chem. Int. Ed.* , 2016, **55**, 2845-2850.
44. A. Eskandari and K. Suntharalingam, A reactive oxygen species-generating, cancer stem cell-potent manganese(II) complex and its encapsulation into polymeric nanoparticles, *Chem. Sci.*, 2019, **10**, 7792-7800.
45. A. Johnson, C. Olelewe, J. H. Kim, J. Northcote-Smith, R. T. Mertens, G. Passeri, K. Singh, S. G. Awuah and K. Suntharalingam, The anti-breast cancer stem cell properties of gold(i)-non-steroidal anti-inflammatory drug complexes, *Chem. Sci.*, 2023, **14**, 557-565.

46. A. Eskandari, A. Kundu, S. Ghosh and K. Suntharalingam, A Triangular Platinum(II) Multinuclear Complex with Cytotoxicity Towards Breast Cancer Stem Cells, *Angew. Chem. Int. Ed.*, 2019, **58**, 12059-12064.
47. G. Dontu, W. M. Abdallah, J. M. Foley, K. W. Jackson, M. F. Clarke, M. J. Kawamura and M. S. Wicha, In vitro propagation and transcriptional profiling of human mammary stem/progenitor cells, *Genes Dev.*, 2003, **17**, 1253-1270.
48. C. Lu, K. Laws, A. Eskandari and K. Suntharalingam, A reactive oxygen species-generating, cyclooxygenase-2 inhibiting, cancer stem cell-potent tetranuclear copper(II) cluster, *Dalton Trans.*, 2017, **46**, 12785-12789
49. A. Degterev, J. Hitomi, M. Germscheid, I. L. Ch'en, O. Korkina, X. Teng, D. Abbott, G. D. Cuny, C. Yuan, G. Wagner, S. M. Hedrick, S. A. Gerber, A. Lugovskoy and J. Yuan, Identification of RIP1 kinase as a specific cellular target of necrostatins, *Nat. Chem. Biol.*, 2008, **4**, 313-321.
50. J. X. Li, J. M. Feng, Y. Wang, X. H. Li, X. X. Chen, Y. Su, Y. Y. Shen, Y. Chen, B. Xiong, C. H. Yang, J. Ding and Z. H. Miao, The B-RafV600E inhibitor dabrafenib selectively inhibits RIP3 and alleviates acetaminophen-induced liver injury, *Cell Death Dis.*, 2014, **5**, e1278-e1278.
51. H. Wang, L. Sun, L. Su, J. Rizo, L. Liu, L. F. Wang, F. S. Wang and X. Wang, Mixed lineage kinase domain-like protein MLKL causes necrotic membrane disruption upon phosphorylation by RIP3, *Mol. Cell*, 2014, **54**, 133-146.
52. D. Chen, J. Yu and L. Zhang, Necroptosis: an alternative cell death program defending against cancer, *BBA - Reviews on Cancer*, 2016, **1865**, 228-236.
53. J. Sosna, S. Voigt, S. Mathieu, A. Lange, L. Thon, P. Davarnia, T. Herdegen, A. Linkermann, A. Rittger, F. K. Chan, D. Kabelitz, S. Schutze and D. Adam, TNF-induced necroptosis and PARP-1-mediated necrosis represent distinct routes to programmed necrotic cell death, *Cell Mol. Life. Sci.*, 2014, **71**, 331-348.
54. X. Xu, C. C. Chua, M. Zhang, D. Geng, C. F. Liu, R. C. Hamdy and B. H. Chua, The role of PARP activation in glutamate-induced necroptosis in HT-22 cells, *Brain Res.*, 2010, **1343**, 206-212.
55. C. K. Donawho, Y. Luo, Y. Luo, T. D. Penning, J. L. Bauch, J. J. Bouska, V. D. Bontcheva-Diaz, B. F. Cox, T. L. DeWeese, L. E. Dillehay, D. C. Ferguson, N. S. Ghoreishi-Haack, D. R. Grimm, R. Guan, E. K. Han, R. R. Holley-Shanks, B. Hristov, K. B. Idler, K. Jarvis, E. F. Johnson, L. R. Kleinberg, V. Klinghofer, L. M. Lasko, X. Liu, K. C. Marsh, T. P. McGonigal, J. A. Meulbroek, A. M. Olson, J. P. Palma, L. E. Rodriguez, Y. Shi, J. A. Stavropoulos, A. C. Tsurutani, G. D. Zhu, S. H. Rosenberg, V. L. Giranda and D. J. Frost, ABT-888, an orally active poly(ADP-ribose) polymerase inhibitor that potentiates DNA-damaging agents in preclinical tumor models, *Clin. Cancer Res.*, 2007, **13**, 2728-2737.
56. M. Banasik, H. Komura, M. Shimoyama and K. Ueda, Specific inhibitors of poly(ADP-ribose) synthetase and mono(ADP-ribosyl)transferase, *J. Biol. Chem.*, 1992, **267**, 1569-1575.
57. S. Burma, B. P. Chen, M. Murphy, A. Kurimasa and D. J. Chen, ATM phosphorylates histone H2AX in response to DNA double-strand breaks, *J. Biol. Chem.*, 2001, **276**, 42462-42467.
58. J. Y. Ahn, J. K. Schwarz, H. Piwnica-Worms and C. E. Canman, Threonine 68 phosphorylation by ataxia telangiectasia mutated is required for efficient activation of Chk2 in response to ionizing radiation, *Cancer Res.*, 2000, **60**, 5934-5936.
59. S. J. Greay, D. J. Ireland, H. T. Kissick, A. Levy, M. W. Beilharz, T. V. Riley and C. F. Carson, Induction of necrosis and cell cycle arrest in murine cancer cell lines by Melaleuca alternifolia (tea tree) oil and terpinen-4-ol, *Cancer Chemother. Pharmacol.*, 2010, **65**, 877-888.
60. M. A. Babcook, R. M. Sramkoski, H. Fujioka, F. Daneshgari, A. Almasan, S. Shukla, R. R. Nanavaty and S. Gupta, Combination simvastatin and metformin induces G1-phase cell cycle arrest and Ripk1- and Ripk3-dependent necrosis in C4-2B osseous metastatic castration-resistant prostate cancer cells, *Cell Death Dis.*, 2014, **5**, e1536.
61. Y. S. Cho, S. Challa, D. Moquin, R. Genga, T. D. Ray, M. Guildford and F. K. Chan, Phosphorylation-driven assembly of the RIP1-RIP3 complex regulates programmed necrosis and virus-induced inflammation, *Cell*, 2009, **137**, 1112-1123.
62. Y. Zhang, S. S. Su, S. Zhao, Z. Yang, C.-Q. Zhong, X. Chen, Q. Cai, Z.-H. Yang, D. Huang, R. Wu and J. Han, RIP1 autophosphorylation is promoted by mitochondrial ROS and is essential for RIP3 recruitment into necrosome, *Nature Commun.*, 2017, **8**, 14329.
63. J. Lu, W. Shi, B. Liang, C. a. Chen, R. Wu, H. Lin, Y. Zhang and J. Han, Efficient engulfment of necroptotic and pyroptotic cells by nonprofessional and professional phagocytes, *Cell Discov.*, 2019, **5**, 39.
64. T. L. Aaes, A. Kaczmarek, T. Delvaeye, B. De Craene, S. De Koker, L. Heyndrickx, I. Delrue, J. Taminau, B. Wiernicki, P. De Groote, A. D. Garg, L. Leybaert, J. Grooten, M. J. Bertrand, P. Agostinis, G. Berx, W. Declercq, P. Vandenabeele and D. V. Krysko, Vaccination with Necroptotic Cancer Cells Induces Efficient Anti-tumor Immunity, *Cell Rep.*, 2016, **15**, 274-287.
65. D. Tang, Y. Yu, J. Zhang, X. Dong, C. Liu and H. Xiao, Self-Sacrificially Degradable Pseudo-Semiconducting Polymer Nanoparticles that Integrate NIR-II Fluorescence Bioimaging, Photodynamic Immunotherapy, and Photo-Activated Chemotherapy, *Adv. Mater.*, 2022, **34**, 2203820.
66. K. A. Papavassiliou, A. A. Sofianidi, V. A. Gogou and A. G. Papavassiliou, Leveraging the ROS–TME Axis for Cancer Treatment, *Antioxidants*, 2024, **13**, 1365.
67. N. Casares, M. O. Pequignot, A. Tesniere, F. Ghiringhelli, S. Roux, N. Chaput, E. Schmitt, A. Hamai, S. Hervas-Stubbs, M. Obeid, F. Coutant, D. Metivier, E. Pichard, P. Aucouturier, G. Pierron, C. Garrido, L. Zitvogel and G. Kroemer, Caspase-dependent immunogenicity of doxorubicin-induced tumor cell death, *J. Exp. Med.*, 2005, **202**, 1691-1701.
68. Q. Wang, X. Ju, J. Wang, Y. Fan, M. Ren and H. Zhang, Immunogenic cell death in anticancer chemotherapy and its impact on clinical studies, *Cancer Lett.*, 2018, **438**, 17-23.
69. A. Terenzi, C. Pirker, B. K. Keppler and W. Berger, Anticancer metal drugs and immunogenic cell death, *J. Inorg. Biochem.*, 2016, **165**, 71-79.
70. A. Tesniere, F. Schlemmer, V. Boige, O. Kepp, I. Martins, F. Ghiringhelli, L. Aymeric, M. Michaud, L. Apetoh, L. Barault, J. Mendiboure, J. P. Pignon, V. Jooste, P. van Endert, M. Ducreux, L. Zitvogel, F. Piard and G. Kroemer, Immunogenic death of colon cancer cells treated with oxaliplatin, *Oncogene*, 2010, **29**, 482-491.
71. X. Huang, Q. Ren, L. Yang, D. Cui, C. Ma, Y. Zheng and J. Wu, Immunogenic chemotherapy: great potential for improving response rates, *Front. Oncol.*, 2023, **13**, 1308681.
72. J. K. Tan and H. C. O'Neill, Maturation requirements for dendritic cells in T cell stimulation leading to tolerance versus immunity, *J. Leukoc. Biol.*, 2005, **78**, 319-324.

View Article Online
DOI: 10.1039/D6QI00611F

Data Availability Statement

The data supporting this article have been included as part of the Supplementary Information.

The structure reported in this article has been deposited with the Cambridge Crystallographic Data Centre (CCDC 2483096). This information can be obtained free of charge from www.ccdc.cam.ac.uk/data_request/cif.